Resonance phenomena in molecular photoionization: impact of synchrotron radiation

R. P. Madden and A. G. Parr

The nature of resonance phenomena in atomic and molecular systems is reviewed along with a discussion of the utilization of synchrotron radiation in studying resonance phenomena. The effects of autoionization and shape resonances on the branching ratios and asymmetry parameters for several systems are discussed. The potential and current status of threshold photoelectron spectroscopy and ion coincidence techniques are discussed.

I. Introduction

The utilization of synchrotron radiation (SR) for the study of atomic, molecular, and solid state physics, beginning in the early 1960s, has had an important impact on these sciences. The high intensity, polarization, and continuous spectral coverage of this unique source of radiation have been effectively utilized to carry out a variety of experiments previously difficult or impossible. In this paper we wish to summarize and illustrate recent advances that have occurred in the study of resonant phenomena in molecular systems.

Historically, the interaction of electromagnetic radiation with isolated atomic and molecular systems has proven to be one of the most useful probes of the internal dynamics of the system. For example, the role of absorption spectroscopy in the development of a quantum mechanical picture of the atom is familiar to every student of quantum mechanics. Systematic studies of the energy and intensity of isolated absorption lines of neutral atoms and molecules have revealed, through appropriate modeling, a consistent quantum mechanical picture of most atomic and molecular phenomena. The use of SR in atomic and molecular physics has been reviewed recently in books[1,2] and by several authors at the Vacuum Ultraviolet Physics Conference in Charlottesville, Virginia in 1980.[3–5]

Resonance phenomena in absorption spectra can occur even above the first ionization limits of the system, where the freed electron can carry away a continuum of possible energies. Such resonances can be due to the creation of a state of the neutral atom or molecule, which involves the excitation of inner electrons or more than one electron simultaneously. This highly excited state can then decay by a variety of mechanisms, such as autoionization, leaving an ion and one or more free electrons; or, in certain cases, it may lead to dissociation.

Another class of resonance phenomena occurs when the effective potential that the electron experiences becomes positive for some range of electron coordinates creating a potential barrier. The positive portion of the effective potential is due to the combination of centrifugal effects and shielding by other electrons. Resonance phenomena of this type are known as shape resonances, i.e., due to the shape of the atomic or molecular potential.

Examples of both autoionization effects and shape resonances will be given below. The effect of shape resonances in molecular photoionization, less widely understood than autoionization, can be quite pronounced. In addition to causing structure in the total cross section, a shape resonance affects the distribution of the vibrational transition amplitudes and the angular distribution of photoelectrons. The Born-Oppenheimer approximation allows a separation of the motion of nuclei and electrons in solving the molecular Hamiltonian. The Franck-Condon factors, which give vibrational amplitudes in molecular electronic transitions, therefore rely on the Born-Oppenheimer approximation in that the amplitude of the electronic transition is assumed to be independent of the vibrational quantum numbers.[6] However, the trapping of a photoexcited electron in the region of the molecule due to a potential barrier allows an exchange of energy and angular momentum between the electron and the nuclei. This coupling of the nuclear and electronic motion results in a breakdown of the Born-Oppenheimer approximation. A recent review of the general topic of resonance phe-

The authors are with U.S. National Bureau of Standards, Synchrotron Ultraviolet Radiation Facility, Washington, D.C. 20234.

Received 21 August 1981.

nomena by Biondi *et al.*[7] discusses the historical aspects of observations of resonances in atomic and molecular systems.

The utilization of SR sources in recent years has allowed rapid advances to be made in the study of these resonance effects. First, the continuous spectral coverge allows the photoionization continuum to be completely examined and the shape of existing resonances to be determined. Second, the very high intensities available mean that there are sufficient photons to do multiple spectroscopies on one system. For example, one can measure photoelectron angular distributions of molecules with resolutions of 0.6 Å for photons, 0.1 eV for electron energies, and 2° angular resolution simultaneously. Third, the polarization of SR allows these distributions to be measured with an increased sensitivity to the asymmetry parameter as discussed in Sec. II.

II. Experimental Measurements

The resonant phenomena to be discussed here will be largely restricted to the study of the following reaction:

$$AB + h\nu(\epsilon) \rightarrow AB^+ + e^-(E,\theta) \quad (1a)$$

$$\rightarrow AB^* \rightarrow AB^+ + e^-(E,\theta), \quad (1b)$$

where AB represents a generalized molecule and e^- the outgoing electron of energy E and direction θ with respect to the polarization ϵ of the light. If the total ionization cross section is to be measured, it is sufficient to measure the intensity of AB^+ as a function of photon energy. This can be done with a mass spectrometer or, lacking a desire for mass selection, by a simple ionization detector. When SR is used as a photon source for studying these reactions, the radiation is highly polarized in the plane of the orbit. The percentage of polarization varies somewhat depending on the optics used, but it is typically 60–80% horizontally polarized when emerging from a normal-incidence monochromator. The differential cross section then can be written

$$\frac{d\sigma_v}{d\Omega} = \frac{\sigma_v}{4\pi}\left\{1 + \frac{\beta}{4}[3P\cos(2\theta) + 1]\right\}, \quad (2)$$

where σ_v = cross section for a particular vibrational channel (assume the molecule is in a ground state initially and ignore rotation);

β = asymmetry parameter;

θ = angle between the electron exit direction and the preferred direction of the electric field of the incident light, measured in a plane normal to the incident light direction; and

P = polarization of light $P = (I_\parallel - I_\perp)/(I_\parallel + I_\perp)$, where $I_\parallel$ is the intensity of the component along the direction $\theta = 0$ and $I_\perp$ is the component at an angle $\theta = 90$. In the situation described here this corresponds to $\theta = 0$ being horizontal.

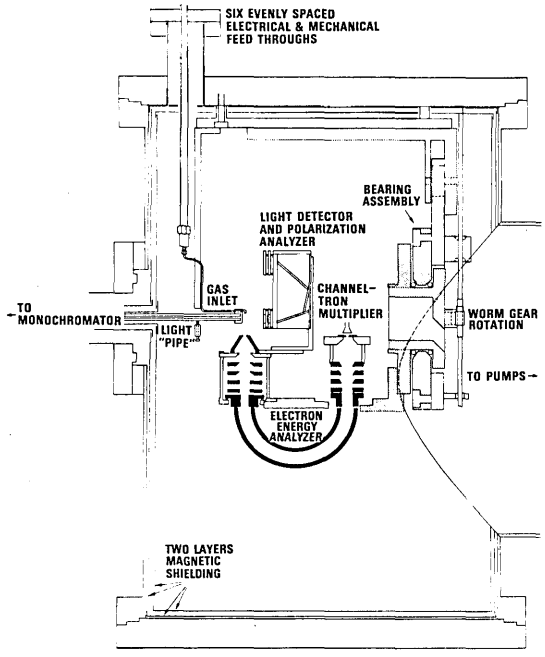

Fig. 1. External view of the rotatable photoelectron spectrometer used at NBS for angle-resolved variable-wavelength photoelectron spectroscopy.

For a review of this equation and its origins, see Ref. 2.

The asymmetry parameter β is a measure of the departure of the angular distribution from a pure $\sin^2\theta$ or $\cos^2\theta$ distribution and is limited to a range $-1 \leq \beta \leq 2$. If, for example, the outgoing electron is a pure p wave, the β parameter is 2. Due to the fact that the outgoing electron wave function is seldom a pure state, β turns out to be a sensitive parameter determined by the mixture of the final state configurations.

The number of electrons measured as a function of angle θ suitably normalized to light flux is proportional to the differential cross section. Hence we can rewrite Eq. (2) as

$$\frac{dN_v}{d\Omega} = \frac{N_v}{4\pi}\left[1 + \frac{\beta}{4}(3P\cos 2\theta + 1)\right]. \quad (3)$$

Here, assuming P is known, β can be determined by measuring the rate of electrons arriving at several different angles. The value of N_v can also be determined, which, for vibrationally resolved work, will give the relative transition amplitudes or branching ratios between the competing (outgoing) vibrational channels.

An instrument developed at NBS to perform these measurements is shown in Fig. 1. This device simultaneously monitors the light intensity and polarization as well as the intensity of electrons as a function of angle. The light from the storage ring has its electric field vector predominantly normal to the plane of the drawing; hence the information necessary to deduce the branching ratios and the asymmetry parameter can be obtained by rotation of the electron energy analyzer through an angle of 90° about the incident light axis.

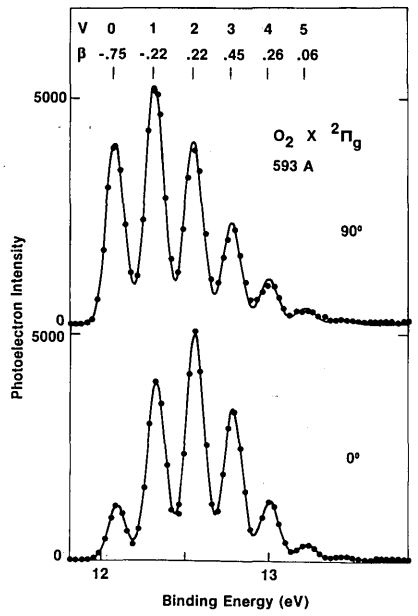

Fig. 2. Two photoelectron spectra of O_2 at 593 Å taken at 0° and 90° with respect to polarization of the light. The ions left in the ground electronic state with the vibrational excitation shown. Change in the relative heights of the same vibrational peak in the two spectra indicates different βs for the various vibrational levels.

The result of a typical measurement using the molecule O_2 as an example is shown in Fig. 2. The difference in the vibrational intensity distribution of the photoelectrons obtained at different angles demonstrates directly a different β for the various vibrational transitions.

III. Autoionization

The alternate reaction indicated in Eq. (1b) represents situations in which the molecular system absorbs the incident photon, momentarily forms a superexcited state, and finally ionizes. When the superexcited state is an electronic excitation of the neutral molecule, this process is called autoionization and manifests as a resonance phenomena in the photoionization continuum. For simplicity, let us first consider this phenomena in atomic systems.

One of the first applications of SR was to use its continuum nature to study in detail photoabsorption of the noble gases at photon energies above their first ionization limits. These first explorations revealed a multitude of discrete resonance structures with a surprisingly strong visibility caused by the existence of high-lying energy levels of the neutral atoms involving the excitation of inner-shell electrons or more than one electron simultaneously.[8] These superexcited states decay quickly (10^{-13}–10^{-14} sec) leaving an ion with the photoelectron carrying away any excess energy. The classic case of two-electron excitation states exists for helium. Figure 3 shows the resonance structure in the photoabsorption of helium at 60.12 eV due to the excitation $1s^2\,{}^1S_0 \rightarrow 2s2p\,{}^1P_1$. Physically the resonance is an interference effect as illustrated in Fig. 4 (taken from

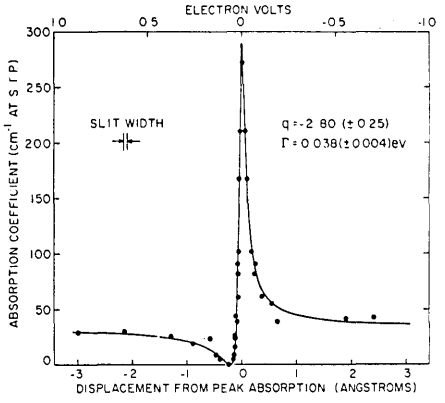

Fig. 3. Absorption profile at the $2s2p\,{}^1P_1$ resonance in He. Dots are the experimental values and the solid line is the theoretical fit with Eq. (4) (Ref. 9).

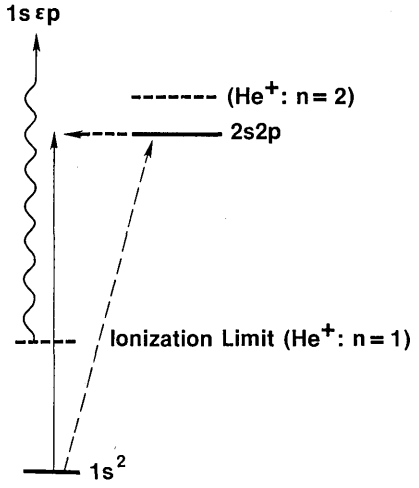

Fig. 4. Schematic representation of the energy levels of He and transitions to levels that can lead to autoionization. The $2s2p$ level is, in the single electron description, a state of neutral He, which is the first member of a series converging on the He^+:$n = 2$ state. This state lies above the ionization limit of He^+ ($1s$), hence it decays via autoionization into the continuum.

Ref. 9). At the energy of the two-electron excitation state the direct ionization process (solid line) is in competition with the excitation to the two-electron excitation state (dashed line). In this simple case of a single level and a single adjacent continuum, the interference between these two excitation channels results in a resonance profile given by

$$\frac{(q+\epsilon)^2}{1+\epsilon^2}, \tag{4}$$

where $\epsilon = \Delta E/\Gamma$,
Γ = halfwidth of the resonance,
ΔE = energy displacement from resonance center,
$q = (\langle\Phi|T|i\rangle)/(\langle\psi_E|T|i\rangle \pi V_E)$,
$\langle\Phi|T|i\rangle$ is the transition matrix element to the (modified) discrete state,

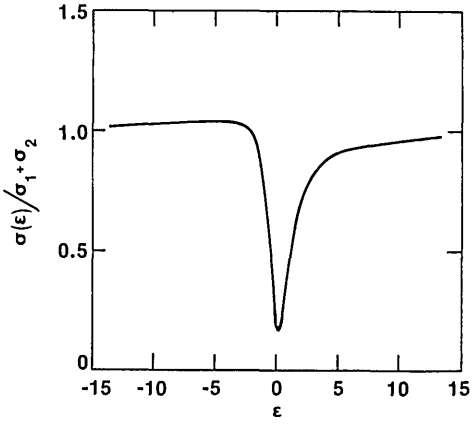

Fig. 5. Theoretical resonance profile fit to observed window absorption resonance due to the $3s^23p^6{}^1S_0 \rightarrow 3s3p^64p^1P_1$ transition in Ar. ϵ is the reduced energy parameter in (4) and the vertical scale is the cross section normalized to the background total cross section.

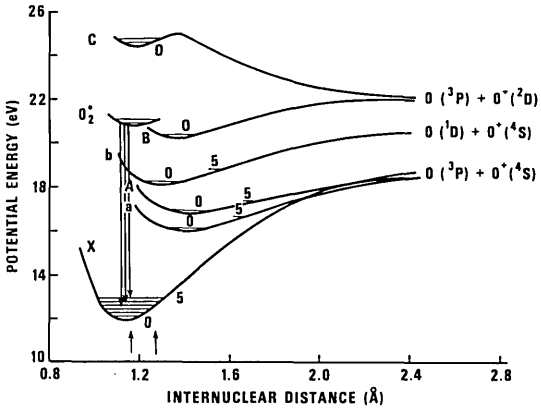

Fig. 6. Potential energy diagram of O_2^+ used to show types of transition possible in molecular photoionization. Curve marked X is the ground state of the ion, a, A, b, B, c are excited ionic states, and the curve marked O_2^* is an excited neutral state that can autoionize.

$\langle \psi_E | T | i \rangle$ is the transition matrix element to the continuum state (in absence of the discrete state), and

V_E is the autoionization matrix element.

The value of q determines the shape of the resonance profile, which can be strongly absorbing, asymmetric, or, for very small absolute values of q, appear as a window in the continuum absorption. q^2 is related to the oscillator strength of the transition to the discrete state in the absence of an interfering continuum.

Inspection of Fig. 3 will show that the He $2s2p$ resonance is clearly asymmetric. An example of a low q (window) resonance is given in Fig. 5 (taken from Ref. 10). Here the autoionizing transition, in Ar[8,10] is a one-electron transition where that electron is excited out of an inner shell. In particular, the discrete transition responsible for this resonance is $3s^23p^6\ {}^1S_0 \rightarrow 3s3p^64p^1P_0$.

The theory of autoionization for atoms is reviewed by Fano and Cooper.[11] Autoionization in molecular photoabsorption spectra is reviewed in the literature.[12,13] The theory for molecular autoionization has been reviewed in Refs. 12 and 14. Recently Raoult and Jungen[15] applied multichannel quantum defect theory to calculate vibration preionization in H_2.

A. Oxygen

Molecular photoionization also shows a wealth of such autoionization structure having both the asymmetric and window profiles. However, in addition to the multiple electronic excitation channels available to atoms, molecules have additional degrees of freedom, namely, vibration and rotation. Hence, the energy partitioning of the final state can be somewhat more complicated than in atoms. Figure 6 shows a simplified family of molecular potential curves for oxygen that demonstrates the types of transitions that can occur. The curve marked X is the ground state of the molecular ion with vibrational energy levels indicated. Transitions can take place to the various levels of this state from the ground state of the neutral molecule. There are, in general, excited states of the ions, indicated by a, A, and b, which also can be photoexcited directly from the neutral ground state. The curve marked O_2^* represents an excited state of the neutral molecule, which has an energy that lies well above the first ionization potential. Once formed, this state can decay into the various electronic–vibrational–rotational states of the ionic system. Loss of energy by radiation to a neutral state is not favored by the relative decay rates.

The relative population of vibrational levels in one electronic transition is governed by the overlap integrals of the initial and final state vibrational wave functions. These overlap integrals (the Franck-Condon factors) are, in the Born-Oppenheimer approximation, independent of the photon energy and dependent only on the relevant molecular potential curves. The presence of an autoionizing level disturbs this picture in that the transition from ground to ionic states is not direct but proceeds through the intermediate state $(AB)^*$. The vibrational transition amplitudes must then include information about the intermediate state $(AB)^*$ and its coupling to the appropriate states of the ion. The importance of autoionization in a molecular spectrum can be seen by looking at the high resolution O_2 spectrum taken by Codling and Madden[16] and shown in Fig. 7.

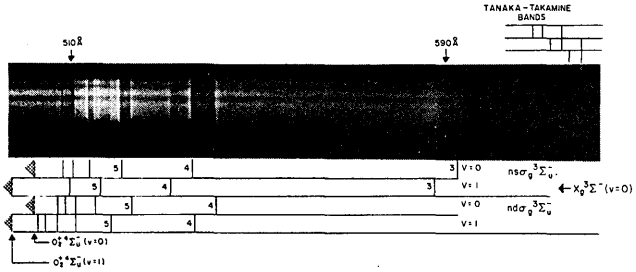

Fig. 7. Absorption spectrum of O_2 in the 500–600-Å region showing autoionization structure with asymmetric window-type resonances.[16] (This is a positive print, therefore black denotes absorption.)

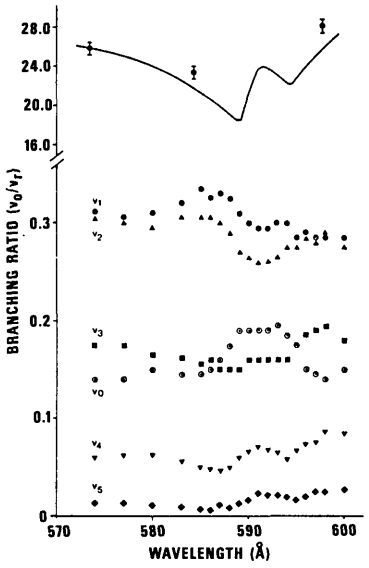

Fig. 8. Branching ratios for various vibrational levels of the O_2^+ ground state extending over the window resonance region of 570–600 Å. (refer to Fig. 5.) Note that the $v = 1$ vibrational level is the most intense. Symbols are defined on the figure.

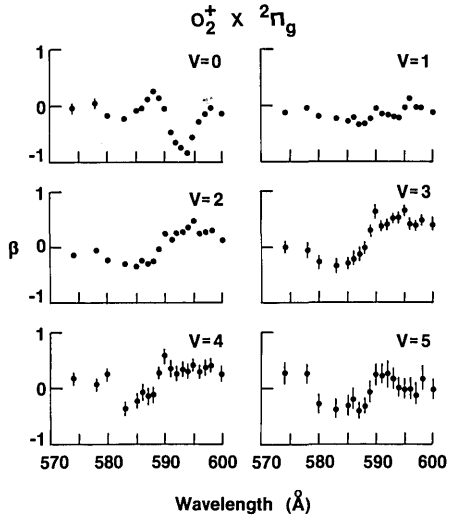

Fig. 9. Asymmetry parameters β for the $v = 0$ through $v = 5$ vibrational levels of the ground state of O_2^+ in the 570–600-Å window resonance region.

Let us now consider the results obtained from the study of angle-resolved photoemission in O_2 as described in Sec. II. The photon energy was scanned over the 575–600-Å region, where O_2 has two close window resonances due to the autoionization of the $V = 0$ and $V = 1$ levels of the $2\sigma_\mu^{-1}3s\sigma$ state of neutral O_2 to the $O_2^+ X^2\Pi_g$ ground state.[17] The results obtained for the branching ratios and βs derived from the photoelectron angular distributions are shown in Figs. 8 and 9. A full report is in Ref. 18. Figure 8 gives the absorption spectra obtained from the literature in the top part of the figure and the branching ratios of the various vibrational levels of the $X^2\Pi_g$ ground state. If there were no resonance phenomena due to the autoionization,

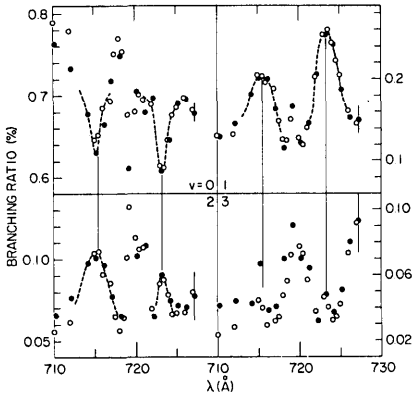

Fig. 10. High-resolution (0.4 Å) branching ratios for the first four vibrational levels of N_2^+ in the 710–730-Å region. Autoionization lines are the absorption and window series converging on the $v = 0$ level of the $B^2\Sigma_u^+$ state of N_2^+. See Ref. 20 for further discussion. Open and closed dots refer to two separate runs.

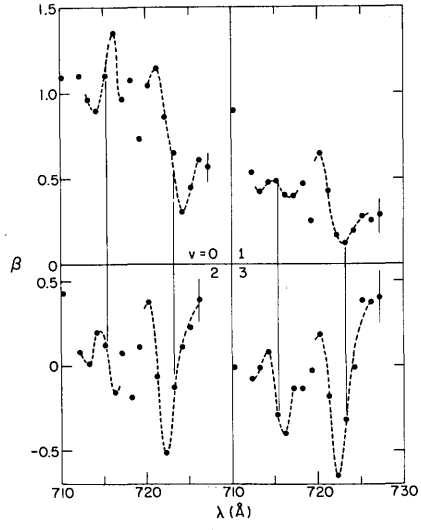

Fig. 11. Asymmetry parameters for $v = 0$ through $v = 3$ levels of the ground state of N_2^+ in the 710-Å region.

these curves would be flat. The β parameter for the $V = 0$ to $V = 5$ vibrational levels of the $X^2\Pi_g$ state are given in Fig. 9. Note that the βs of the various vibrational levels undergo different changes in the resonance region. The asymmetry parameter is a function of the phases and amplitudes of the outgoing continuum wave functions. The variance of β with vibrational levels implies a coupling of the electronic and nuclear motion, which is at variance with the Born-Oppenheimer separation. The breakdown of the Born-Oppenheimer approximation results in the Franck-Condon principle no longer being directly applicable.

B. Nitrogen

The results of an angular distribution study of photoelectrons while scanning the incident photon energy through isolated (resolved) autoionization resonances in N_2 are shown in Figs. 10 and 11. The 710–730-Å

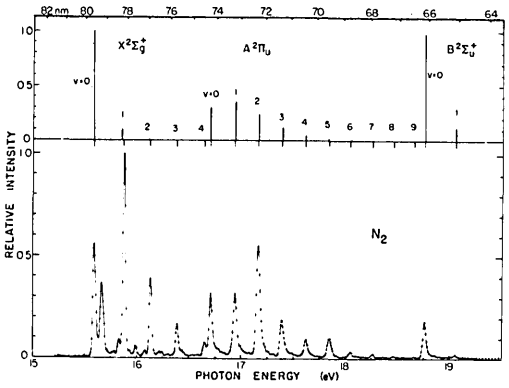

Fig. 12. Threshold photoelectron spectrum for molecular nitrogen. Bottom portion is the threshold photoelectron spectrum and at the top is a histogram of the Franck-Condon factors. Note the anomalous intensity ratios.

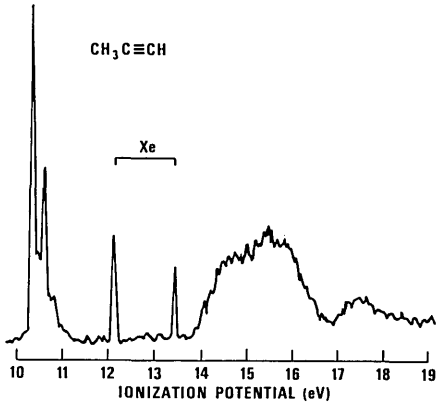

Fig. 13. Photoelectron spectra of propyne from Ref. 23. Vertical scale is total electron counts. Horizontal scale is electron kinetic energy adjusted to show the binding energy of the electrons. This PES spectrum was taken with a He 584-Å excitation source.

wavelength region is in the region of the Hopfield emission and absorption series.[19] The data in the two figures are for the photoelectrons that leave the N_2 ion in the $X^2\Sigma_g^+$ ground state. Again, as in O_2, the branching ratios change through the resonances, and the changes are different for the various vibrational members of the series. The asymmetry parameters shown in Fig. 11 undergo large changes going through the resonances. These observations again indicate the breakdown of the simple models of molecular ionization and offer an important and waiting area for theoretical development. A full report on N_2 is given in Ref. 20.

IV. Autoionization and Threshold Photoelectron Spectra

Threshold photoelectron spectroscopy (TPES) has been developed over the years as a tool to study the energetics of molecular ion fragmentation.[21] These experiments involve photoionization followed by the collection of those electrons that leave the interaction with essentially zero energy (hence threshold processes) as a function of photon energy. An extension of the experiment is to collect ions in coincidence with the threshold electron and measure the ratio of the various coincident ions as a function of photon energy. Figure 12 shows the TPES of N_2.[22] The lower portion is the measured TPES and the upper portion a histogram of the calculated Franck-Condon factors. Note the general disagreement on the relative amplitudes of the transitions to the various electronic–vibrational levels. As in the other work discussed here, rotational levels are not resolved. The difference in the intensities is ascribed to autoionization, in which the internal energy is left in the molecule and the electron does not carry off the excess energy. This process has been given the name degenerate autoionization.

The implications for energy input into molecules during ionization are significant. The degenerate autoionization process leaves internal energy in the molecule, which in turn can contribute to fragmentation. This is particularly important in polyatomic molecules, where a large amount of excess energy can be stored in the various vibrational modes. For theoretical modeling it is highly desirable to study fragmentation as a function of internal energy. TPES allows a known amount of internal energy to be deposited. However, in many molecular ions the electronic states are sufficiently separated that there are energy regions in which there are no directly accessible states. These regions, often called Franck-Condon gaps, would be difficult to study using TPES and ion coincidence techniques if it were not for the degenerate autoionization process.

In a threshold electron-ion coincidence experiment the relative rate of ion formation is measured as a function of energy. Since the photoelectron carries away no appreciable energy, the excess energy is deposited in internal energy of the molecular ion. The ratio of the number of ions of a given type to the total number of ions as a function of internal energy is called the breakdown curve. The collection of these curves for a given molecule constitutes the basic ingredients for comparison with the statistical theory of molecular dissociation.[23]

As an example of this situation, let us consider the molecule propyne, which has a structural formula $CH_3 - C \equiv C - H$. This molecule has been studied by 584-Å photoelectron spectroscopy.[24] Figure 13 shows the PES of propyne. Note that in the 11.5–13.75-eV region there are very few photoelectrons. Figure 14 shows the results of a TPES experiment and a study of the fragment ions by coincident ion detection.[25] Figure 14(A) is the TPES obtained by measuring the number of threshold photoelectrons as a function of wavelength. Figure 14(B) is the ratio of the number of coincident ions of a particular mass to the total number of coincident ions. Since only threshold electrons are detected, the horizontal scale is the internal energy of the molecular ion; i.e., subtracting the ionization potential gives the actual energy stored in the system. At ~11.5 eV the internal energy is such that the $C_3H_4^+$ ion starts losing an H atom. As the stored energy increases above 11.5 eV, the proportion of $C_3H_4^+$ then increases, and eventually all the $C_3H_4^+$ formed by the initial ionization subsequently decays into fragment states. At still higher energies

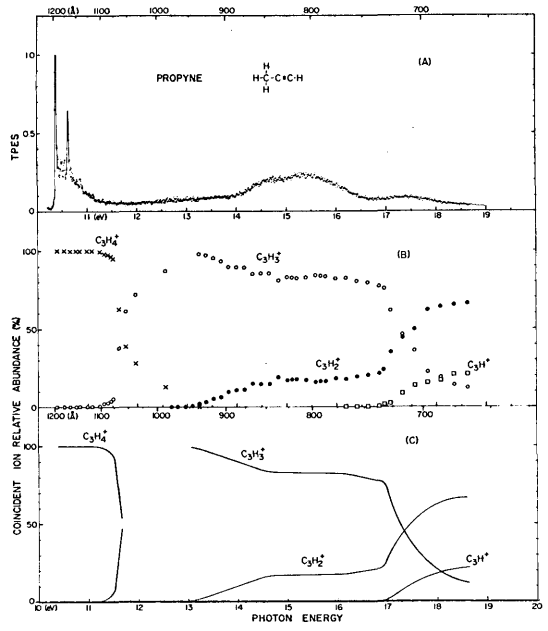

Fig. 14. This figure gives (A) threshold photoelectron spectra as a function of energy, (B) data obtained in the threshold photoelectron–photoion coincidence experiment that gives the breakdown curves, and (C) a computer fit to (B) showing smooth breakdown curves. Region between 11.6 and 12.8 eV has been left off the computer fit due to uncertainties in interpretation.

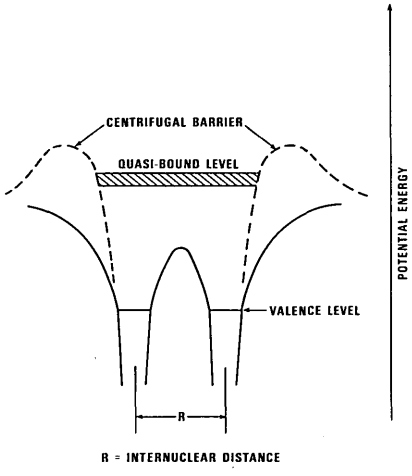

Fig. 15. Schematic idealization of the electronic potential for a hypothetical diatomic molecule, which shows the origin of a shape resonance. For high angular momentum, the centrifugal term combined with electron screening effects can make the effective potential positive, resulting in a potential barrier.

other processes start occurring, such as $C_3H_2^+$ formation and C_3H^+ formation. Figure 12(C) represents a smooth fit to the data. The region between 11.5 and 12.5 eV is left out due to uncertainties in interpretation.

The important observation is that the region between 11.5 and 13.75 eV in the PES shows a Franck-Condon gap. The existence of autoionization in the region results in the formation of excited states of the ion, which allows this type of study to proceed. If it were not for the degenerate autoionization, no ions would have been detected in this region.

Recently, Connerade *et al.* used the Bonn synchrotron to perform high-resolution absorption studies on selected organic molecules. Their spectra indicate the existence of autoionization in the Rydberg levels of the molecules they studied.[26] The continued use of SR in threshold photoelectron-coincident-photoion studies will prove to be a fruitful and informative area of study for the future. Work has already begun at the ACO storage ring in Orsay, France, using a coincident-ion detection apparatus.[27] The availability of high-flux monochromators at SR sites will allow the measurements outlined here to be more easily obtained. Further, it will be possible to start studying in detail the effects of higher-energy radiation on the fragmentation process. This will involve the study of the excitation of atomiclike core levels in the molecules and how such absorbed energy may or may not be transmitted to vibrational modes.

V. Shape Resonances

Shape resonance effects oocur in a wide range of molecular ionization phenomena, with a significant impact on vibrational branching ratios and angular distributions. Why shape resonances occur in molecules can be understood in terms of the schematic shown in Fig. 15. Calculations demonstrate that at certain energies and for certain channels of molecular photoionization, high angular momentum components of the electron contribute to the outgoing wave. These high angular momentum components contribute to a centrifugal term in the effective potential, which when added to the attractive term can result in a local positive effective potential maxima. This positive barrier can have the effect of temporarily trapping the electron in the region of the ion core.[28] The temporary trapping of the excited electron results in a coupling of the electronic motion with that of the nuclear motion. As a consequence, the Franck-Condon conditions are violated, and the branching ratios of the various vibrational transitions and the angular distributions of the photoelectrons are affected. The phenomena are now known to be widespread in molecular photoionization, having been recently reported for diatomic molecules (see Secs. IV.A–C) and also for polyatomic molecules such as acetylene[29] and sulfur hexafluoride.[30]

A. Nitrogen

A shape resonance affecting the distribution of vibrational transition intensities in N_2 photoionization was predicted by Dehmer *et al.*[31] in the $3\sigma_g$ photoionization channel. The effect of this shape resonance has been seen by West *et al.*[32] and is shown in Fig. 16. The data points represent the experimentally determined ratio of the $V = 1$ to $V = 0$ transition amplitudes in the $X^2\Sigma_g^+$ state of N_2^+. The triangles are data obtained by Gardner and Samson.[33] The solid line represents a calculation by Dehmer *et al.*[31] using the multiple scattering model they developed. This model allows an estimation of the effects of a shape resonance on vi-

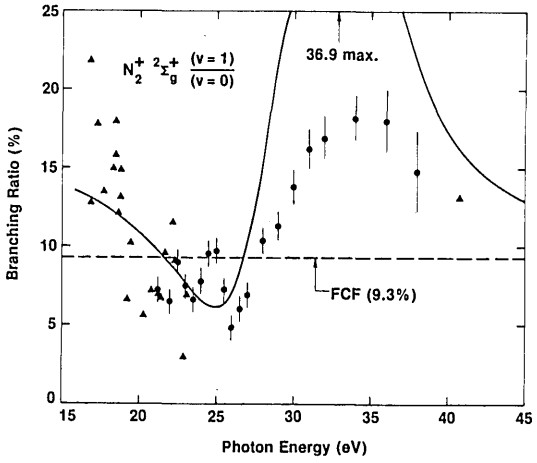

Fig. 16. Branching ratios as a function of energy for production of the $V = 0,1$ levels of $N_2^+ X^2\Sigma_g^+$ by photoionization of N_2: ●, Ref. 32; ▲, Ref. 33; —, theory from Ref. 31; - - -, Franck-Condon factor of 9.3% (D. L. Albritton, 1979; private communication).

brational transitions and of a vibrationally dependent asymmetry parameter. The dashed horizontal line is the calculated Franck-Condon factor. The scatter in the data below 22 eV is probably due to the presence of autoionization effects; however, the broad resonance stretching over 20 eV is certainly the predicted shape resonance effect. The general shape of the data is as predicted by the theory, with some overestimating the strength of the shape resonance effect, due perhaps to lack of inclusion of mechanisms such as electron correlation which may damp the structure. Recently, Krummacher *et al.*[34] reported on inner-shell photoionization in N_2. They studied the effects of electron correlation as well as the potential-well shape resonances. An important conclusion of their work is that electron correlations have to be taken into account in a direct manner to correctly account for observations.

B. Carbon Monoxide

CO is isoelectronic to N_2 and as such is expected to exhibit a shape resonance effect on the photoelectron angular distributions and vibrational branching ratios. Figure 17 shows the experimentally determined branching ratios for CO, and Fig. 18 shows the experimentally determined asymmetry parameters.[35,36] The branching ratios for the $V = 1/V = 0$ show the same general structure as observed for N_2 but over a somewhat contracted region. The Franck-Condon factor for this is ~3.8%. The other thing to note is that the Franck-Condon factors for the $V = 2$ and $V = 3$ states are very small, and these states normally do not appear in the photoelectron spectra. However, in the region of the shape resonance, transitions resulting in these final states take on a measurable amplitude. The βs for the various vibrational channels behave differently as a function of photon energy as seen in Fig. 18, and the variation in β is largest for the weaker vibrational transitions. The origin of the structure below 20 eV is uncertain.

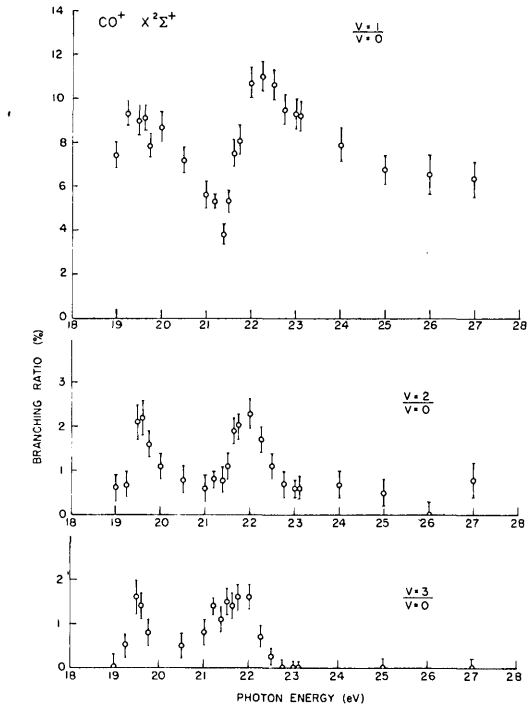

Fig. 17. Vibrational branching ratios of $CO^+ X^2\Sigma^+$ state resulting from photoionization of the CO ground state. Branching ratios are normalized to the $V = 1$ level. Structure above 21 eV is thought to be due to a shape resonance. Data from Ref. 35.

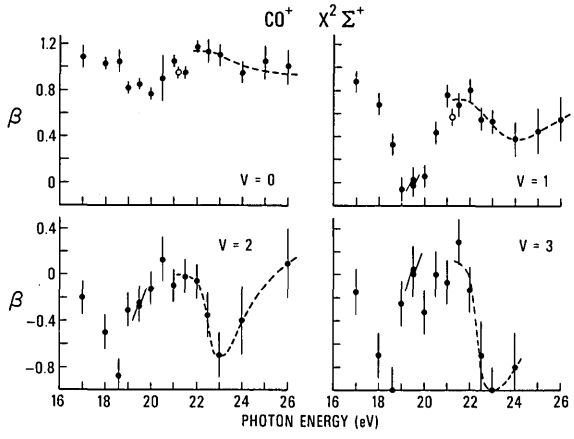

Fig. 18. Asymmetry parameter β for the first four vibrational levels of the CO^+ ground state resulting from photoionization of the CO ground state. Data from Ref. 36.

Recent theoretical work by Dill and Dehmer[37] shows the general trend in βs and branching ratios for CO as indicated here. The interpretive situation is complicated by the existence of double-electron excitations in CO in this energy region.

C. Other Molecules

Shape resonance phenomena are now recognized in the total absorption cross section and in the vibrationally unresolved branching ratio studies and angular

distributions of a number of molecules. There are results on O_2,[6,38] SF_6,[39] C_2H_2,[29] and CO,[40] that show the effect of shape resonances. New results obtained by the NBS group in molecular dynamics indicates that shape resonance effects are important in a wide range of molecular photoionization phenomena—a conclusion supported by recent theoretical work by Dill and Dehmer.[37]

VI. Conclusions

The resonance effects discussed here have been unveiled largely due to the availability of synchrotron radiation sources. The continuous spectral coverage, polarization, and high intensity available with SR have all been utilized in the experimental achievement of high-resolution angle-resolved photoelectron spectroscopy of molecules. Such sources are today becoming readily available. The national synchrotron light source (NSLS) at Brookhaven National Laboratory will have at least one beam line devoted to gas-phase atomic and molecular physics. The Aladdin storage ring at Stoughton, Wis. will have gas-phase beam lines. Internationally, the storage ring ACO in Orsay, France, is already active in this field, and the storage rings in Berlin, West Germany (BESSY), and at Daresbury, England, will have beam lines devoted to gas-phase experiments. These will be in addition to the experiments already in progress at current storage-ring facilities.[41]

The photoelectron spectroscopic techniques described here and the mass spectrometric techniques already available will soon be combined to study resonance effects on fragmentation processes. In addition, the study of the formation of multiple-charge states formed by direct processes or resonance phenomena will be an important area of investigation.[42] The use of techniques to study photon-stimulated molecular fluorescence is an important aspect not covered in detail here. Fluorescent measurements add complementary information to that obtainable by measurement of only the charged species in photoionization. For example, an excited molecular ion can lose energy by radiation and as a consequence have less energy available for bond breakage or a rearrangement process. In addition, a study of the polarization of the fluorescence gives symmetry information that is very helpful in identifying the final state composition.[43]

The important role of resonance phenomena in elucidating the effects of electron interaction and correlation effects in atoms has been recognized for many years. Due to the availability of intense SR sources, it appears that the study of similar resonance phenomena in molecular systems will be equally rewarding.

We would like to acknowledge the contributions of our co-workers: Keith Codling, Barry Cole, Joe Dehmer, Dave Ederer, Roger Stockbauer, and John West. In addition, useful discussions with Henry Rosenstock are appreciated.

References

1. C. Kunz, Ed. *Synchrotron Radiation; Technique and Applications*, (Springer, Berlin, 1979), see particularly the chapters by Codling and by Koch and Sonntag.
2. H. Winick and S. Doniach, Ed. *Synchrotron Radiation Research* (Plenum, New York, 1980), see chapter by M. Krause, pp. 101–151.
3. J. B. West, Appl. Opt. **19,** 4063 (1980).
4. P. M. Guyon and I. Nenner, Appl. Opt. **19,** 4068 (1980).
5. V. Schmidt, Appl. Opt. **19,** 4080 (1980).
6. G. Herzberg, *Molecular Structure and Molecular Spectra I: Spectra of Diatomic Molecules* (Van Nostrand Reinhold, New York. 1980).
7. M. A. Biondi, A. Herzenberg, and C. E. Kuyatt, Phys. Today **32,** 44 (1979).
8. R. P. Madden and K. Codling, Phys. Rev. Lett. **10,** 516 (1963).
9. R. P. Madden and K. Codling, Astrophys. J. **141,** 369 (1965).
10. R. P. Madden, D. L. Ederer, and K. Codling, Phys. Rev. **177,** 136 (1969).
11. U. Fano and J. W. Cooper, Rev. Mod. Phys. **40,** 441 (1968).
12. J. A. R. Samson, "Atomic Photoionization," in *Handbuch der Physik, Vol. 31*, W. Mehlhorn, Ed. (Springer, Berlin), in press.
13. J. Berkowitz, *Photoabsorption, Photoionization and Photoelectron Spectroscopy* (Academic, New York, 1979).
14. T. Rescigno, V. McKoy, and B. Schneider, *Electron Molecule and Photon Molecule Collisions* (Plenum, New York, 1978).
15. M. Raoult and C. Jungen, J. Chem. Phys. **74,** 3388 (1981).
16. K. Codling and R. P. Madden, J. Chem. Phys. **42,** 3935 (1965).
17. P. M. Dehmer and W. Chupka, J. Chem. Phys. **62,** 4525 (1975); W. S. Watson and J. Moiton, At. Data Nucl. Data Tables **22,** 103 (1978).
18. K. Codling, *et al.*, J. Phys. B **14,** 657 (1981).
19. J. J. Hopfield, Phys. Rev. **35,** 1133 (1930); **36,** 789 (1930).
20. A. C. Parr *et al.*, Phys. Rev. Lett. **46,** 22 (1981); J. B. West, K. Codling, A. C. Parr, D. L. Ederer, B. E. Cole, R. Stockbauer, and J. L. Dehmer, J. Phys. B **14,** 1791 (1981).
21. See discussion in Ref. 12. For application in synchrotron radiation see Ref. 4.
22. R. Stockbauer, J. Chem. Phys. **70,** 2108 (1979); W. B. Peatman, B. Gotcher, P. Gurtler, E. E. Koch, and V. Saile, J. Chem. Phys. **69,** 2089 (1978).
23. H. M. Rosentock, M. B. Wallenstein, A. L. Wahrhaftig, and H. Eyring, Proc. Natl. Acad. Sci. U.S.A. **38,** 607 (1952).
24. D. C. Frost, F. G. Herring, C. A. McDowell, and Z. A. Stenhouse, Chem. Phys. Lett. **4,** 533 (1970).
25. A. C. Parr, A. J. Jason, R. Stockbauer, K. E. McCulloh, Int. J. Mass. Spectrom. Ion Phys. **30,** 319 (1979).
26. J. P. Connerade, M. A. Baig, and S. P. McGlynn, J. Phys. B **13,** 167 (1981).
27. See Ref. 6 and references therein.
28. See P. W. Langhoff in Ref. 13 and J. L. Dehmer and D. Dill in Ref. 13 for a current theoretical picture of shape resonance phenomena.
29. R. Unwin, I. Kban, N. V. Richardson, A. M. Bradshaw, L. S. Cederbaum, and W. Domcke, Chem. Phys. Lett **77,** 242 (1981).
30. T. Gustafsson, Phys. Rev. A **18,** 1481 (1978); L. C. Lee, E. Phillips, and D. L. Judge, J. Chem. Phys. **67,** 1237 (1977).
31. J. L. Dehmer, D. Dill, and S. Wallace, Phys. Rev. Lett. **43,** 1005 (1979).
32. J. B. West, A. C. Parr, B. E. Cole, D. L. Ederer, R. Stockbauer, and J. L. Dehmer, J. Phys. B **13,** L105 (1980).
33. J. L. Gardner and J. A. R. Samson, J. Electron Spec. **13,** 7 (1918).
34. S. Krummacher, V. Schmidt, and F. Wuilleumier, J. Phys. B: **13,** 3993 (1980) (also a review of the N_2 problem).
35. R. Stockbauer, B. E. Cole, D. L. Ederer, J. B. West, A. C. Parr, J. L. Dehmer, Phys. Rev. Lett. **43,** 757 (1979).

36. B. E. Cole, *et al.* J. Chem. Phys. **72,** 6308 (1980).
37. D. Dill and J. L. Dehmer, Argonne; private communication.
38. P. Morin, I. Nenner, P. M. Guyon, I. Dutuit, and K. Ito, J. Chim. Phys. Phys. Chim. Biol. **77,** 605 (1980).
39. T. Gustafsson, Phys. Rev. A **18,** 1481 (1978).
40. E. W. Plummer, T. Gustafsson, W. Gudat, and D. E. Eastman, Phys. Rev. A **15,** 2339 (1977).
41. For a review and data on storage rings in operation, see Refs. 2 and 3.
42. T. Masuka and J. A. R. Samson, J. Chim. Phys. Phys. Chim. Biol. **77,** 623 (1980).
43. E. D. Poliakoff, J. L. Dehmer, D. Dill, A. C. Parr, K. H. Jackson, and R. W. Zare, Phys. Rev. Lett. **46,** 907 (1981).

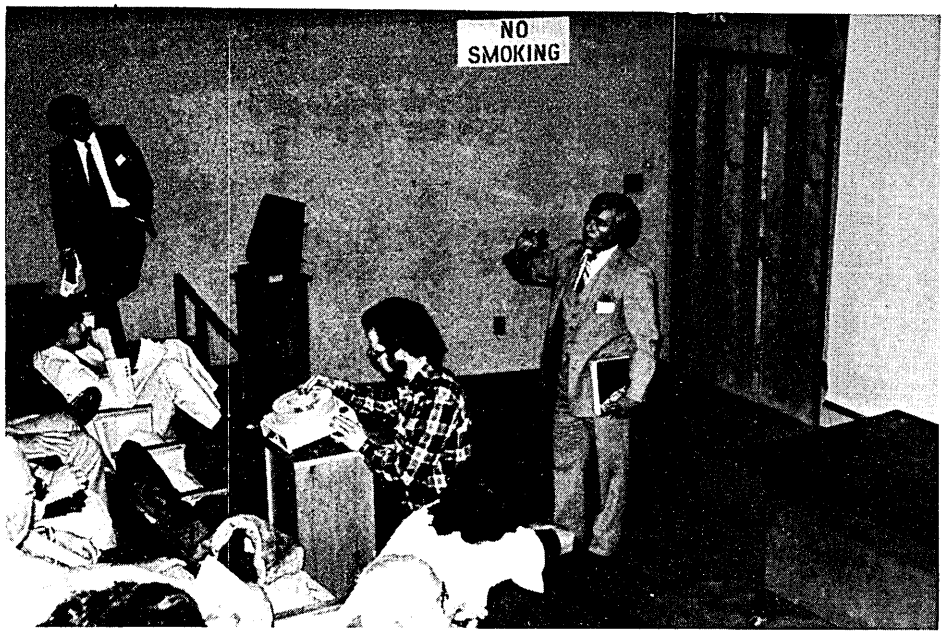

Robert Madden (NBS) photographed by R. Straka answering questions; H. Sakai (U. Mass.) leans against the far back wall.